Spectrochimica Acta Part A: Molecular and Biomolecular Spectroscopy 154 (2016) 220–231

Contents lists available at ScienceDirect

Spectrochimica Acta Part A: Molecular and Biomolecular Spectroscopy

journal homepage: www.elsevier.com/locate/saa

Synthesis characterization and luminescence studies of gamma irradiated nanocrystalline yttrium oxide

N.J. Shivaramu [a], B.N. Lakshminarasappa [a,*], K.R. Nagabhushana [b], Fouran Singh [c]

[a] Department of Physics, Jnanabharathi Campus, Bangalore University, Bangalore 560 056, India
[b] Department of Physics (S & H), PES University, Bangalore 560085, India
[c] Inter University Accelerator Centre, P.O. Box No. 10502, New Delhi 110 067, India

ARTICLE INFO

Article history:
Received 28 February 2015
Received in revised form 22 August 2015
Accepted 26 September 2015
Available online 30 September 2015

Keywords:
Combustion synthesis
Radiation effects
FE-SEM
Electron spin resonance
Photoluminescence
Thermoluminescence

ABSTRACT

Nanocrystalline Y_2O_3 is synthesized by solution combustion technique using urea and glycine as fuels. X-ray diffraction (XRD) pattern of as prepared sample shows amorphous nature while annealed samples show cubic nature. The average crystallite size is calculated using Scherrer's formula and is found to be in the range 14–30 nm for samples synthesized using urea and 15–20 nm for samples synthesized using glycine respectively. Field emission scanning electron microscopy (FE-SEM) image of 1173 K annealed Y_2O_3 samples show well separated spherical shape particles and the average particle size is found to be in the range 28–35 nm. Fourier transformed infrared (FTIR) and Raman spectroscopy reveals a stretching of Y–O bond. Electron spin resonance (ESR) shows V^- center, O_2^- and Y^{2+} defects. A broad photoluminescence (PL) emission with peak at ~386 nm is observed when the sample is excited with 252 nm. Thermoluminescence (TL) properties of γ-irradiated Y_2O_3 nanopowder are studied at a heating rate of 5 K s^{-1}. The samples prepared by using urea show a prominent and well resolved peak at ~383 K and a weak one at ~570 K. It is also found that TL glow peak intensity (I_{m1}) at ~383 K increases with increase in γ-dose up to ~6.0 kGy and then decreases with increase in dose. However, glycine used Y_2O_3 shows a prominent TL glow with peaks at 396 K and 590 K. Among the fuels, urea used Y_2O_3 shows simple and well resolved TL glows. This might be due to fuel and hence particle size effect. The kinetic parameters are calculated by Chen's glow curve peak shape method and results are discussed in detail.

1. Introduction

Nanoparticles (NPs) are great scientific interest because they act as a bridge between bulk materials and atomic or molecular structures. A bulk material exhibits a steady state of physical properties regardless of its size. But, at the nanoscale, this is often not the case due to quantum confinement and/or high surface to volume ratio. High surface to volume ratio reduces the melting temperature of NPs. The properties of NPs can be modified by engineering their size, morphology and composition. It has been shown that various properties such as electrical, mechanical, optical, magnetic, etc. are highly influenced by the fine grained structure with improved properties. Quantum confinement of electrical carriers within NPs plays a vital role in transfer of energy and charge over nanoscale [1]. The materials on such scale have attracted many researchers in various fields of material science, biological science, etc. [2,3]. Currently the importance of nanomaterials in the field of luminescence has been increased. They have potential application such as display materials, tricolor lamps, solar energy converters, sensors, optical amplifier and thermoluminescent dosimeters [2–4].

Numerous techniques such as sol gel [5], co-precipitation [6], solid state reaction [7], hydrothermal [8] and solution combustion [9–11] have been reported for synthesis of nanomaterials. Among these, solution combustion method has greater advantages since it produces crystalline materials at low temperature with high surface to volume ratio. In addition, it has other advantages like high purity, homogeneity, control over stoichiometry and substitution of desired amount of dopants. It has been reported that, the luminescence properties of the as-formed nanoparticles are dependent on the nature of the fuel used in combustion method as it controls the particle size and morphology of the combustion products [12].

Mukherjee et al., studied the morphology and luminescence properties of combustion synthesized Y_2O_3:(Eu,Dy,Tb) nanoparticles using various fuels namely, glycine, phenyl alanine, arginine, glutamic and aspartic acids. They observed that glycine and arginine based nanoparticles exhibit smooth surface and improved luminescence properties when compared to those prepared using other amino acids (fuels) [12]. Ramakrishna et al. reported the effect of different fuels viz diformyl hydrazine (DFH), sugar and urea on structural, photo and thermoluminescence properties of combustion synthesized Y_2SiO_5 nanopowders. SEM micrographs of DFH fuel used sample showed almost spherical shape with agglomerated particles. The TL intensity is found to be higher in DFH used samples when compared to sugar and urea used

* Corresponding author.
E-mail address: bnlnarasappa@rediffmail.com (B.N. Lakshminarasappa).

http://dx.doi.org/10.1016/j.saa.2015.09.019
1386-1425/

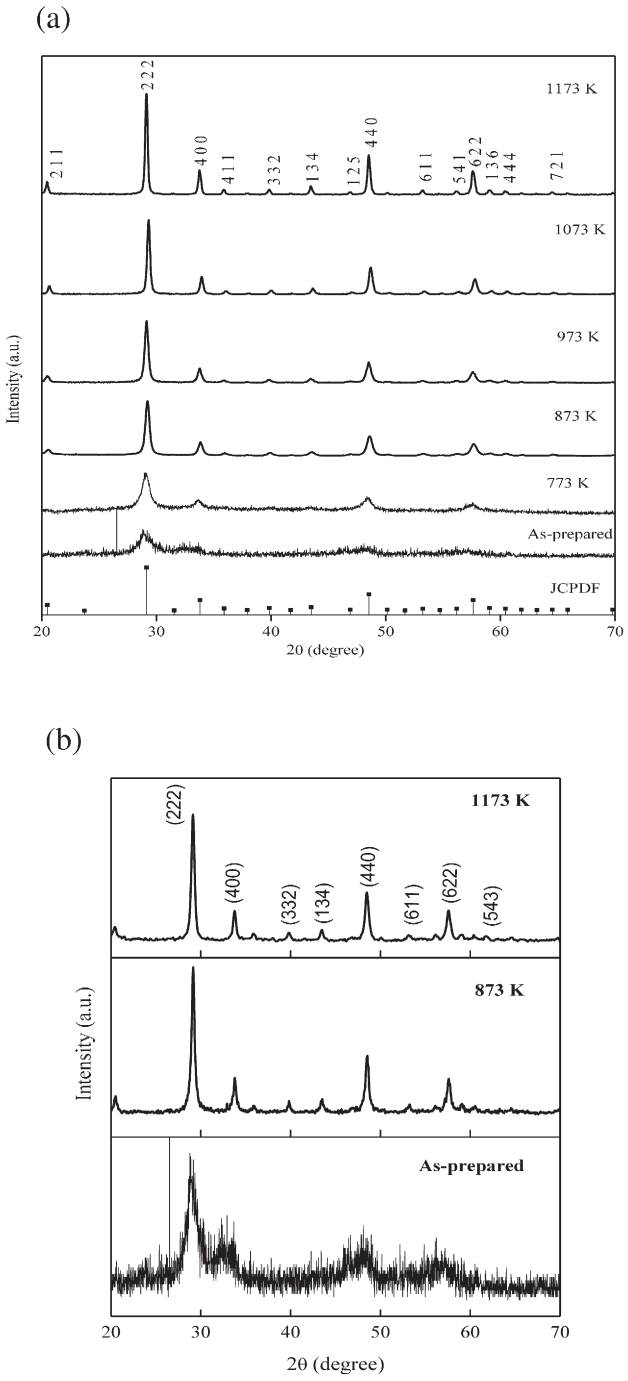

Fig. 1. (a) XRD patterns of U:Y_2O_3 as a function of annealing temperature. (b) XRD patterns of G:Y_2O_3 as a function of annealing temperature.

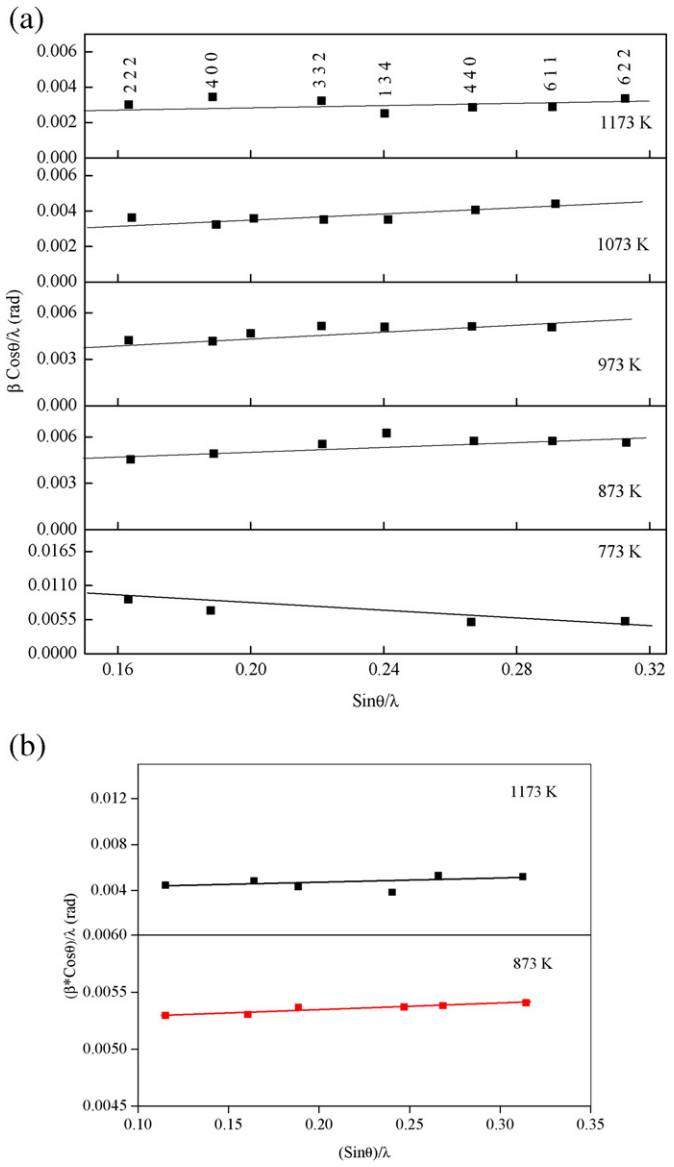

Fig. 2. (a) W–H plot for the combustion synthesized pure U:Y_2O_3. (b) W–H plot for the combustion synthesized pure G:Y_2O_3.

samples under UV and gamma irradiation. They concluded that DFH used Y_2SiO_5 indicates better dosimetric properties [13]. However, efforts are still being made for improving the TL dosimetric properties by using different fuels. TL technique has attracted many researchers from all over the world since this technique is simple and finds wide applications in various fields such as radiation therapy, space research, geology, archeology and other related areas [14–16].

Table 1
XRD structural parameters of U:Y_2O_3 and G:Y_2O_3 annealed at different temperatures.

Fuels	Annealed temperature (K)	Crystallite size (D) (nm)		Lattice constant a, (Å)	Cell volume (Å^3)	Density, ρ (gm cm^{-3})	Dislocation Density δ ($\times 10^{15}$)	Inter-planar space in at. (222) (Å)	Lattice strain (%)	
		Debye Scherer	W–H method						W–H method	Calculated
Urea	773	14.40	10.54	10.590	1187.68	5.052	4.823	3.057	−0.74	0.339
	873	16.68	25.13	10.596	1189.80	5.042	3.594	3.059	0.34	0.176
	973	18.94	26.82	10.603	1192.06	5.033	2.788	3.061	0.28	0.163
	1073	24.50	32.46	10.609	1193.95	5.025	1.666	3.062	0.22	0.140
	1173	29.42	37.31	10.612	1195.07	5.020	1.155	3.063	0.08	0.117
Glycine	873	15.2	19.1	10.590	1187.68	5.052	4.33	3.057	0.09	0.21
	1173	19.2	25.0	10.596	1189.80	5.042	2.71	3.059	0.07	0.18

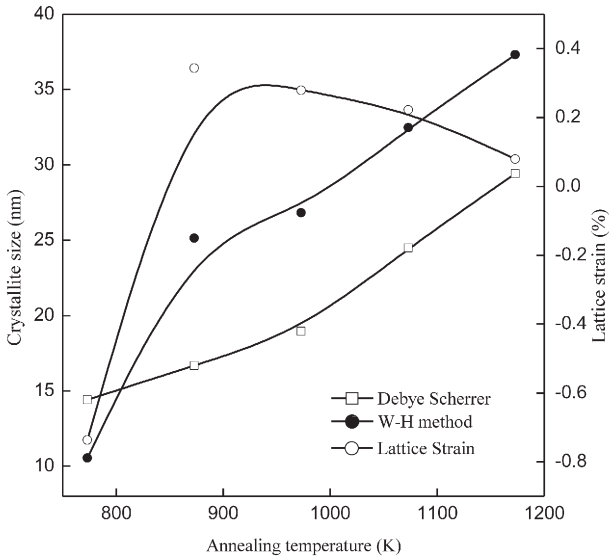

Fig. 3. Variation of crystallite size and lattice strain with annealing temperature.

Yttrium oxide (yttria) finds potential application because of its high corrosion resistivity and thermal stability. Y_2O_3 possess high refractory properties, high melting point (~2723 K) and a high thermal conductivity (33 W m^{-1} K^{-1}). It is a suitable material for photonic waveguide due to its high band gap (5.72 eV) with a very high refractive index (~2) and in a wide transmission range (280–8000 nm) which is well suited for waveguide applications, dosimeter and good host for display materials [5]. In the present work, Y_2O_3 nanopowders are synthesized by solution combustion technique using urea and glycine as fuels. The obtained nanopowders are characterized using X-ray diffraction (XRD), Field emission scanning electron microscopy (FE-SEM), Fourier transform infrared (FTIR) spectroscopy and Raman spectroscopy. In addition gamma irradiated PL and TL properties of as prepared and annealed Y_2O_3 samples are reported. The TL trapping parameters are calculated by using glow curve shape method.

2. Material and methods

2.1. Preparation of nanocrystalline Y_2O_3

Nanocrystalline yttrium oxide (Y_2O_3) is synthesized by combustion technique, using yttrium nitrate hexahydrate (YN) as an oxidizer, urea and glycine as fuels. Yttrium nitrate hexahydrate ($Y(NO_3)_3 \cdot 6H_2O$) with 99.8% purity procured from Aldrich chemicals, urea (CH_4N_2O)

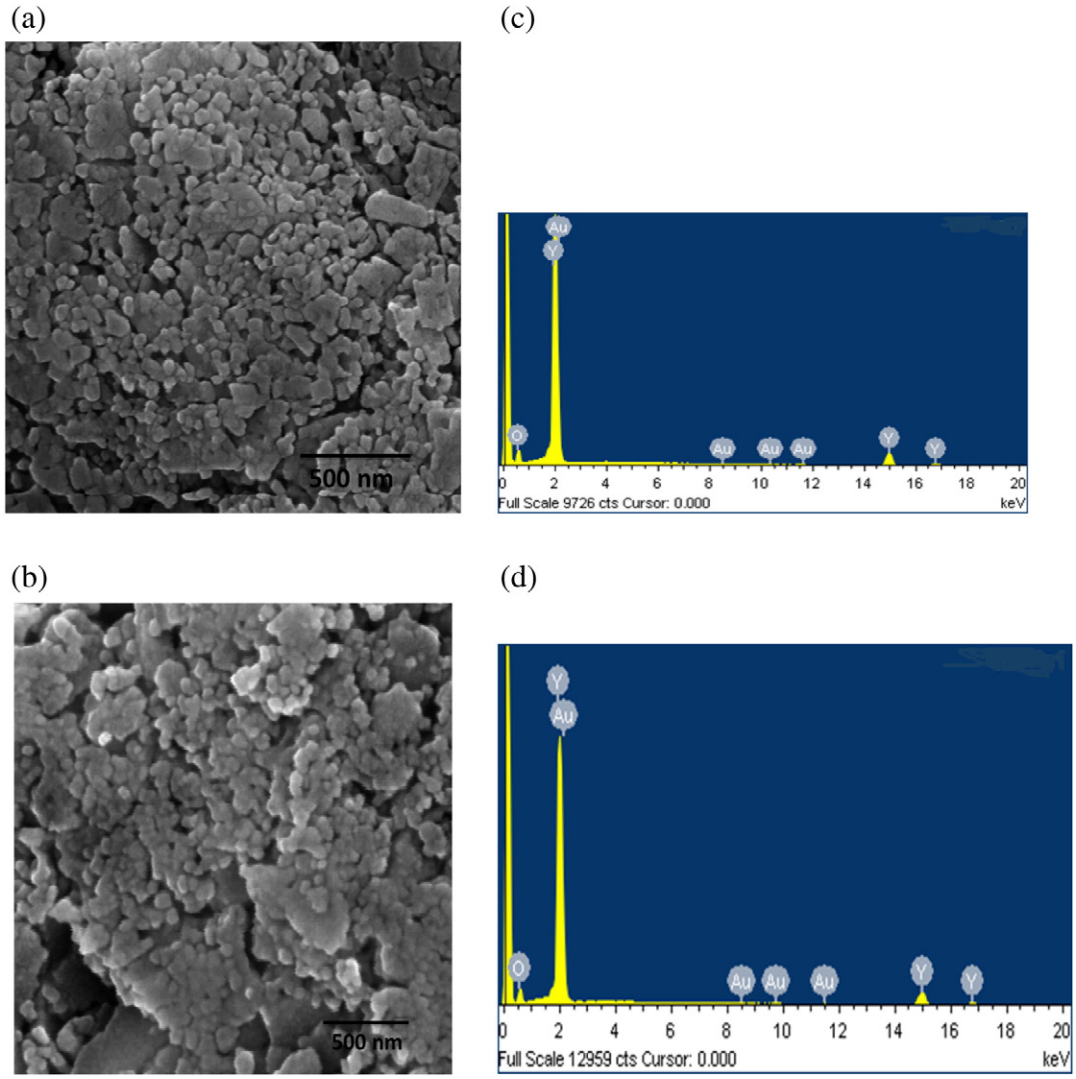

Fig. 4. (a) SEM image of 1173 K annealed U:Y_2O_3. (b) SEM image of 1173 K annealed G:Y_2O_3. (c) EDS of 1173 K annealed U:Y_2O_3. (d) EDS of 1173 K annealed G:Y_2O_3.

with 99.5% purity and glycine ($C_2H_5NO_2$) with 99.7% are procured from Merck specialties private limited. All the chemicals are directly used without any purification. The stoichiometric amounts of yttrium nitrate hexahydrate and urea/glycine are dissolved in a 50 ml of double distilled water in a cylindrical pyrex dish of approximately 600 ml capacity. The homogeneous mixture is introduced into a muffle furnace maintained at 773 ± 5 K. Initially, the solution boils and undergoes dehydration followed by decomposition with evaporation of a large amount of gases leaving behind the powder. The final product is voluminous and whitish [11]. The stoichiometric balanced equations are as follows;

YN : Urea

$$2Y(NO_3)_3 + 5(NH_2)_2CO \rightarrow Y_2O_3 + 5CO_2 + 10H_2O + 8N_2$$

~ 23.0 moles of gases/mol of Y_2O_3

YN : Glycine

$$6Y(NO_3)_3 + 10C_2H_5NO_2 \rightarrow 3Y_2O_3 + 20CO_2 + 25H_2O + 14N_2$$

~ 19.67 moles of gases/mol of Y_2O_3.

As prepared samples are annealed at 773, 873, 973, 1073 and 1173 K for 2 h. Both as synthesized and annealed samples are subjected to the following characterizations. Y_2O_3 samples prepared by using urea and glycine are named as U:Y_2O_3 and G:Y_2O_3 respectively.

2.2. Characterization

As prepared and annealed samples of Y_2O_3 nanoparticles are characterized by X-ray diffraction (XRD), Bruker D8, using Cu-K_α radiation of wavelength 1.5406 Å. The morphology of the synthesized samples is coated with gold and then studied by field emission scanning electron microscopy (FE-SEM) [MIRA II LMH from TESCAN]. Fourier transform infrared (FTIR) spectra of as prepared and annealed Y_2O_3 are recorded using Nicollet spectrophotometer. Raman spectra are recorded in the range 100–1000 cm^{-1} using a Renishaw 1000 Raman spectrometer with an excitation wavelength of 514.5 nm from 0·5 mW of Ar ion laser as excitation source. Y_2O_3 samples are irradiated with γ-rays using ^{60}Co gamma source at room temperature. ESR measurement is carried out using a Bruker X-band continuous wave EMX spectrometer operating at 9.392 GHz. Gamma irradiated nanocrystalline Y_2O_3 sample is attached to a quartz sample holder by ESR-silent Teflon tape. ESR spectrum is recorded at room temperature. Diphenyl picryl hydrazyl (DPPH) is used for calibrating the g-values of defect centers. PL excitation and emission spectra of as prepared, annealed and gamma irradiated Y_2O_3 are recorded using a Hitachi F-2700 fluorescence spectrophotometer. TL measurements are performed at a heating rate of 5 K s^{-1} using a Harshaw-3500 TLD reader. For each TL measurement, 12 mg of γ-ray irradiated sample is used. All experiments are performed at room temperature.

3. Result and discussion

3.1. X-ray diffraction

Fig. 1(a) and (b) shows the XRD patterns of as prepared and annealed Y_2O_3 prepared using urea and glycine respectively. It is observed that, the as prepared U:Y_2O_3 is amorphous in nature. Whereas, samples annealed at 773 K exhibits poor crystalline state characterized by broad diffraction peaks and 873 K annealed samples show complete crystalline phase. Further, as prepared G:Y_2O_3 is also poor crystalline in nature, whereas, 873 K and 1173 K annealed samples show complete crystalline phase. All the observed diffraction peaks are assigned to different (hkl) planes of cubic crystal system with space group $Ia\bar{3}$ using JCPDS: No: 88-1040 [17,18]. It is observed that, the enhancement of crystallinity with increasing annealing temperature i.e. the intensity of the diffraction peaks increases and is become sharper. The crystallite size 'D' of the sample is calculated using Scherrer's Eq. (1),

$$D = \frac{0.9\lambda}{\beta \cos\theta} \quad (1)$$

where, 'D' is the crystallite size, 'λ' is the wavelength of X-rays (1.5406 Å), 'β' is the full width at half maxima (FWHM) and 'θ' is the Bragg angle. The average crystallite size is found to be in the range 14–30 nm and 15–20 nm for U:Y_2O_3 and G:Y_2O_3 respectively. The crystallite size increases with annealing temperature and is tabulated in Table 1. It is clearly seen that 1173 K annealed G:Y_2O_3 shows less crystallite size when compared to U:Y_2O_3 due to less flame temperature

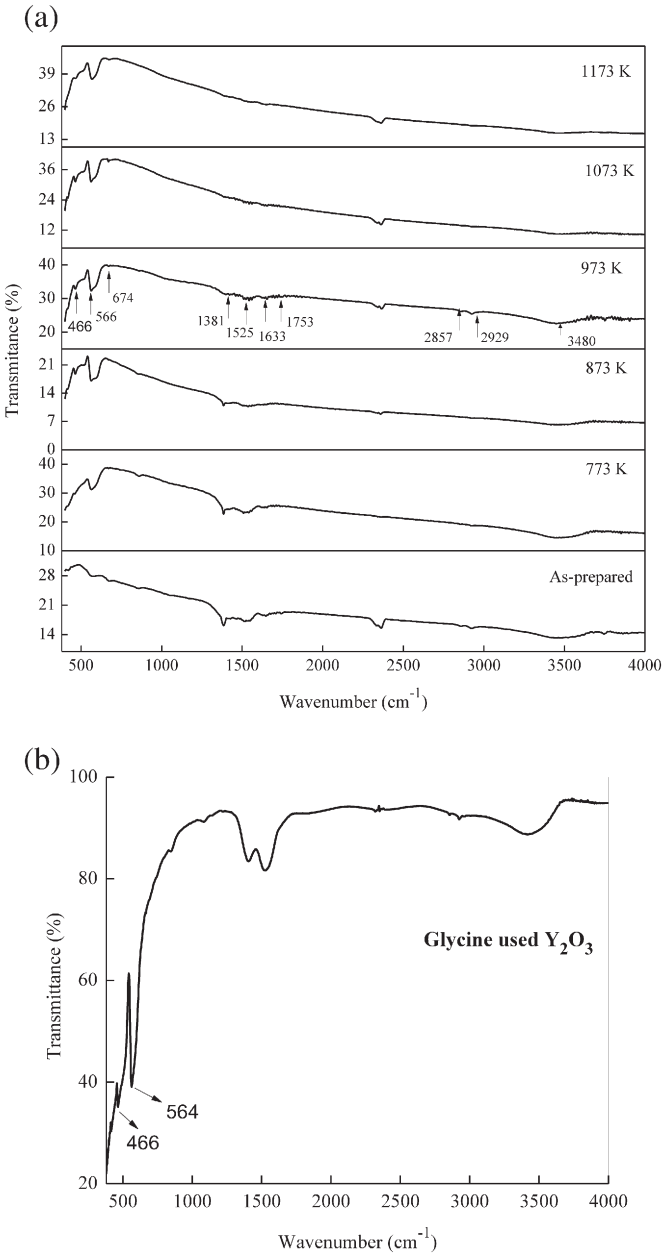

Fig. 5. (a) FT-IR spectra of combustion synthesized U:Y_2O_3. (b) FT-IR spectra of combustion synthesized G:Y_2O_3.

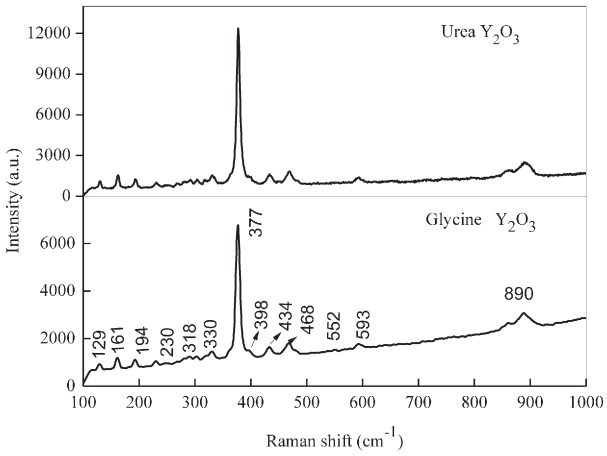

Fig. 6. Raman spectra of 1173 K annealed U:Y_2O_3 and G:Y_2O_3.

during combustion [19]. The lattice strain and crystallite size are estimated using Williamson–Hall (W–H) equation [20],

$$\frac{\beta\cos\theta}{\lambda} = \frac{1}{D} + \frac{4\varepsilon\sin\theta}{\lambda} \quad (2)$$

where, 'ε' is the lattice strain. Fig. 2(a) and (b) shows the plot of β cosθ/λ versus 4sin θ/λ. Here we will get a straight line with a slope equal to the value of the lattice strain and y-axis intercept equal to the inverse of the crystallite size. The average crystallite size is found to be in the range 10–37 nm and 19–25 nm for U:Y_2O_3 and G:Y_2O_3 samples respectively. The average crystallites size is found to increase with increase in annealing temperature. 773 K annealed U:Y_2O_3 samples show negative strain due to lattice shrinkage [21], whereas 873, 973, 1073 and 1173 K annealed samples show positive lattice strain due to tensile strain [22]. It is found that the crystallite size increases while the lattice strain decreases with increase of annealing temperature and is given in Table 1. Variation of crystallite size and the lattice strain with annealing temperature is shown in Fig. 3. It is observed that, the lattice strain increases up to 873 K and then decreases with further increase of annealing temperature for U:Y_2O_3 samples.

The XRD structural parameters namely lattice constant (a), lattice volume (V), inter-planer space (d), density (ρ), dislocation density (δ) and lattice strain (ε) are calculated using the following formulae [22],

$$\rho = \frac{16M}{Na^3} \quad (3)$$

$$\delta = \frac{1}{D^2} \quad (4)$$

$$\varepsilon = \frac{\beta\cos\theta}{4} \quad (5)$$

where, 'M' is the molecular mass, 'N' is the Avogadro's number. The density, dislocation density and lattice strain are calculated and tabulated in Table 1. It shows that the density and dislocation density of the samples decreases with increase of annealing temperature due to enhancement of crystallite size and lattice constant while the inter planer spacing increases with increasing annealing temperature for U:Y_2O_3 and G:Y_2O_3 samples respectively.

3.2. FE-SEM micrograph analysis

FE-SEM is an important tool for studying the topography and surface morphology of the synthesized nanopowders. It is well known that, combustion synthesized product is highly influenced by fuel to metal-ligand complex formation. Depending on the nature of fuel, fuel to oxidizer ratio, the nature of combustion that differs from flaming to non-flaming reactions involves liberation of enormous amount of gases. The pores and voids can be attributed to the large amount of gases escaping out of the reaction mixture during combustion. Fig. 4(a) shows the FE-SEM image of 1173 K annealed U:Y_2O_3 and it is observed that the particles are loosely agglomerated with spherical in nature and voids due to the evolution of large amount of gases during combustion process. And, the average particle size is found to be ~35 nm. Fig. 4(b) shows the FE-SEM image of 1173 K annealed G:Y_2O_3 and it is observed that the particles are agglomerated with spherical shape and the average particle size is found to be 28 nm [12,13]. In the present work, a large number of moles of gas are liberated in combustion process with urea when compared to glycine [19,23]. This indicates that, particles are loosely agglomerated as observed in U:Y_2O_3 due to greater amount of gases escaping during combustion reaction.

The composition of the sample is estimated through energy dispersive X-ray spectroscopy (EDS) technique. It is proved to be a powerful tool to obtain the elemental composition ratio [24] as shown in Fig. 4(c) and (d) for U:Y_2O_3 and G:Y_2O_3 samples annealed at 1173 K. We can see only the element peaks of Y and O in the sample. The concentration of Y and O in the sample is 37.10, 33.48 and 62.90, 66.52 at.% for U:Y_2O_3 and G:Y_2O_3 samples respectively.

3.3. FTIR and Raman spectra analysis

Fig. 5(a) shows the FTIR spectra of as prepared and 773, 873, 973, 1073 and 1173 K annealed U:Y_2O_3 samples. FTIR peak observed at 566 cm^{-1} is attributed to the stretching of Y–O bond [5,23]. The peaks at 674, 854 and 1381, 1525 cm^{-1} are attributed to C–O bond bending [25] and C–O bond stretching, the peaks at 1633 and 1753 cm^{-1} are due to C = O stretching [25,26]. These absorption peaks indicate the presence of carbonate groups. FTIR spectra are recorded using KBr pellet technique. KBr is mixed with the samples to make a very thin pellet and the pellet absorbs CO_2 present in the atmosphere. Hence, FTIR spectra exhibit C–O and related bonds. These results are well reported [5,27]. The peaks at the 2857 and 2929 cm^{-1} are attributed to the O–H bond and 3480 cm^{-1} broad peak indicates that stretching mode of O–H from the moisture is present on the surface of the powder [27]. When the annealing temperature increases, the peak intensity of O–H band gradually decreases and other peak intensities also decrease except 566 cm^{-1}. FTIR spectra of 1173 K annealed sample show a sharp and intense peak at 566 cm^{-1} corresponding to Y–O stretching. This might be due to increase in crystallinity of sample and the results are correlated with XRD patterns. However, 1173 K annealed G:Y_2O_3 shows absorption with peaks at 466 and 564 cm^{-1} and it is attributed to the stretching of Y–O bond as shown in Fig. 5(b) [25,26].

Raman spectroscopy is a very sensitive technique and it provides vibration of molecules within the scattering volume. The representation of optical modes in cubic Y_2O_3 is given [28] as

$$\Gamma_{op} = 4A_g + 4E_g + 14F_g + 5A_{zu} + 5E_u + 16F_u$$

where $4A_g$, $4E_g$ and $14F_g$ are Raman active, $16F_u$ is IR active and $5A_{zu}$ and $5E_u$ are inactive modes. Thus, there are twenty two Raman active

Table 2
Peak positions of Raman modes of 1173 K annealed Y_2O_3.

Peak position (cm^{-1})	129	161	181	194	230	318	330	377	398	434	468	552	567	593
Modes	F_g	$F_g + A_g$	F_g	E_g	F_g	F_g	F_g	F_g	F_g	F_g	F_g	A_g	E_g	F_g

modes, where E_g and F_g modes are doubly and triply degenerated respectively. The Raman active modes of cubic Y_2O_3 can be divided into fifteen modes ($3A_g + 3E_g + 9F_g$) coming from the vibration of O ions and seven modes ($A_g + E_g + 5F_g$) coming from the vibration of Y ions [29]. Fig. 6 shows the room temperature Raman spectrum of 1173 K annealed U:Y_2O_3 and G:Y_2O_3 samples. In Raman modes observed at 129, 161, 181, 194, 230, 318, 330, 377, 398, 434, 468, 552, 567 and 593 cm^{-1} that is a total of fourteen out of twenty two Raman active modes of these, the 377 cm^{-1} shows high scattering intensity. These peak positions are attributed to different modes of vibration as cited in Table 2. Fig. 6 shows that U:Y_2O_3 has high scattering intensity compared to G:Y_2O_3, it might be due to effect of crystallite size [30].

3.4. Electron spin resonance

Electron spin resonance (ESR) is a convenient technique to study the extrinsic and intrinsic defects in samples. Fig. 7 shows the ESR spectrum of 6 kGy γ-irradiated U:Y_2O_3 recorded at room temperature. The ESR spectrum exhibits a weak and unresolved broad signal in the range 2980–3507 G and these signals having peaks at g = 2.002, 2.050 and 2.083 are might be due to V^- center, O_2^- and Y^{2+} defects respectively [31–33]. Wang et al. reported ESR signals in the range 3000 to 3500 G and assigned to unshared electron pair in nanocrystalline Y_2O_3 caused by surface defects originated from metal ions [32]. Osada et al. reported ESR signal with g = 2.070 and 2.003 due to O_2^- and V^- center respectively [31].

3.5. UV–visible spectra

UV–Vis spectra of Y_2O_3 nanoparticles prepared by urea and glycine are shown in Fig. 8(a). Two absorption peaks one at ~252 nm and other at ~ 295 nm are recorded. The ~252 nm absorption is attributed to band gap of Y_2O_3 [3] and 295 nm absorption is attributed to surface traps/defect states. The optical band gap energy (E_g) is estimated using Wood and Tauc relation [34] i.e., $(\alpha h\nu) = K\,(h\nu - E_g)^{1/n}$, where 'hν' is the photon energy, 'α' is the optical absorption coefficient, 'K' is constant and 'n' is dependent on the optical transition with an assigned value of 2 and 1/2 for direct allowed and indirect allowed transitions respectively. Fig. 8(b) is obtained by plotting $(\alpha h\nu)^2$ versus 'E' in the high absorption range. For direct allowed transition, energy gap E_g is found to be 5.2 eV and 5.1 eV for U:Y_2O_3 and G:Y_2O_3 by extrapolating the linear region of the plot to $(\alpha h\nu)^2 = 0$, if $\alpha \neq 0$. This indicates that the allowed direct transition is responsible for the inter-band transition in Y_2O_3 [32].

3.6. Photoluminescence

Fig. 9(a) shows the excitation spectrum of 1173 K annealed U:Y_2O_3. This shows a broad band with peak at 252 nm by monitoring emission at 386 nm. The broad excitation band is due to charge transfer of O^{2-} to Y^{3+} in Y_2O_3 [35,29]. Fig. 9(b) shows the PL emission spectra of as prepared and annealed U:Y_2O_3, under 252 nm excitation. All the samples exhibit a broad emission band in the range 320–600 nm, with peaks at about 386, 440, 468, 486 and 538 nm. Bordun studied the influence of oxygen vacancies in the luminescence spectra of Y_2O_3 [36]. He concluded that, the luminescence bands with peaks at 365 and 428 nm might be due to the presence of oxygen vacancies related to radiative recombination. Osipov and coworkers studied luminescence of pure yttria [37]. They reported cathodoluminescence with peaks in the range 435–510 nm and the emission is ascribed due to recombination of associative Y^{3+}–O^{2-} donor acceptor pair. The reported luminescence peaks are matching with the present work. In present work, the PL emission with peaks at 386 nm may be attributed to oxygen vacancy defects such as F-centers. And, the emissions with peaks at 440, 468 and

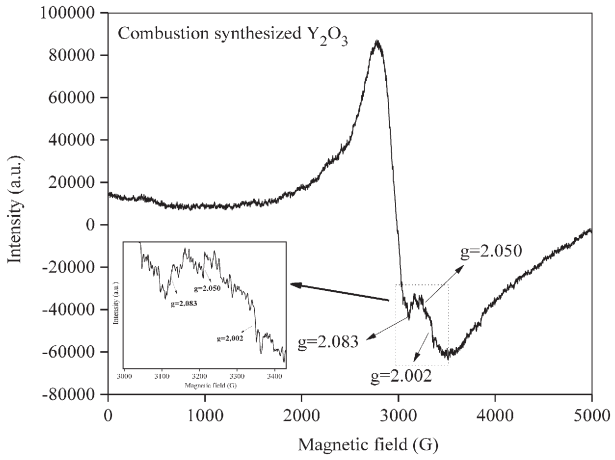

Fig. 7. ESR spectra of 6.0 kGy, γ-irradiated U:Y_2O_3.

538 nm are attributed to Y^{3+}–O^{2-} donor acceptor pair. PL result indicates that the emission intensity of the as prepared sample is very low when compared to those annealed ones. Further, it is found that the emission intensity increases with increasing annealing temperature as

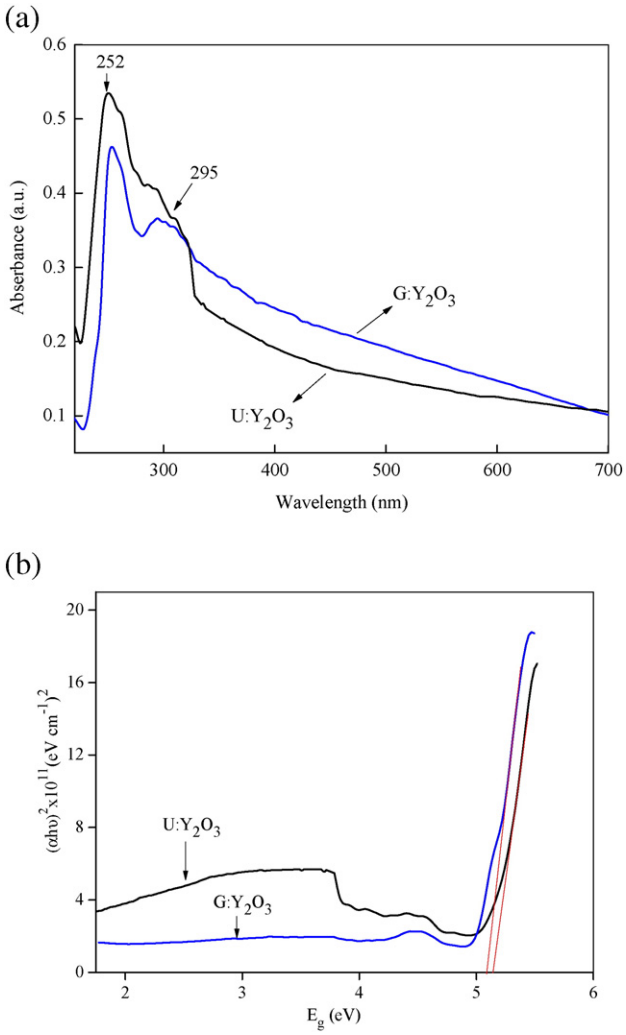

Fig. 8. (a) UV–Vis absorption spectra of U:Y_2O_3 and G:Y_2O_3. (b) Optical energy band gap of U:Y_2O_3 and G:Y_2O_3.

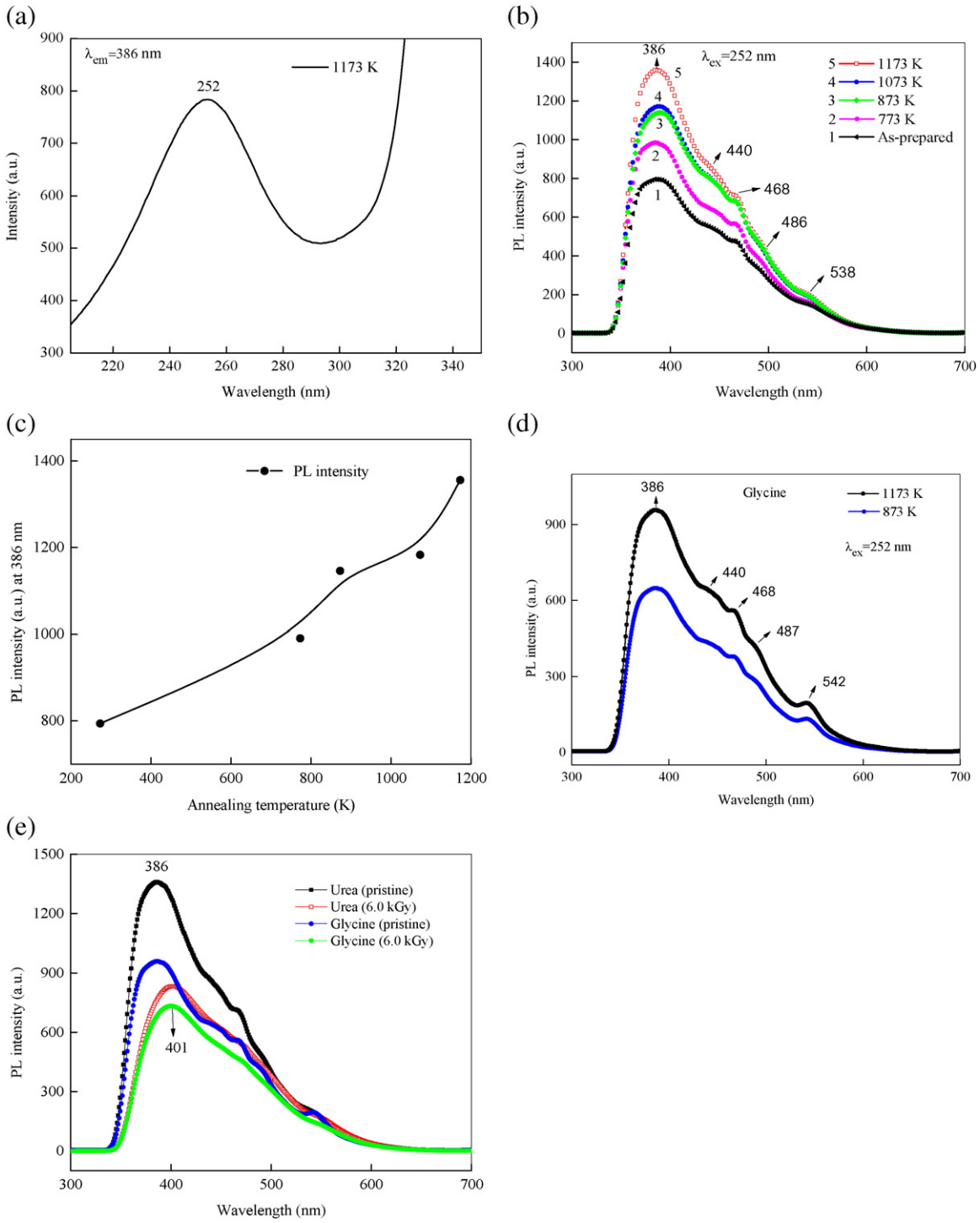

Fig. 9. (a) Photoluminescence excitation spectrum ($\lambda_{em} = 386$ nm) of 1173 K annealed Y_2O_3. (b) Photoluminescence spectra ($\lambda_{ex} = 252$ nm) of U:Y_2O_3. Variation of PL intensity at 386 nm with temperature. (d) PL spectra ($\lambda_{ex} = 252$ nm) of G:Y_2O_3 annealed at different temperatures. (e) PL spectra ($\lambda_{ex} = 252$ nm) of pristine and 6.0 kGy γ-irradiated U:Y_2O_3 and G:Y_2O_3.

can be seen from Fig. 9(c) [38]. This might be due to increase in crystallite size. The growth of crystallite size reduces the non-radiative transition and also the vibration of –OH and C = O impurities, results in the increase of the PL emission intensities [39].

Fig. 9(d) shows the PL emission spectra of 873 and 1173 K annealed G:Y_2O_3. All the samples exhibit a broad emission band in the range of 350–600 nm. It clearly seen that PL emission peaks are similar to those observed in U:Y_2O_3. However, PL intensity is observed to be higher in U:Y_2O_3 when compared to G:Y_2O_3 probably due to enhancement of crystallinity [39].

Fig. 9(e) shows the PL emission spectra of 1173 K annealed pristine and gamma irradiated Y_2O_3 upon 252 nm excitation. The PL intensity of U:Y_2O_3 and G:Y_2O_3 is found to decrease in 6.0 kGy gamma irradiated samples. This might be due to higher concentration of defects that generates nonradiative states caused by high energy gamma photons with a higher dose rate in the forbidden gap [40–42]. The PL emission (386 nm) peak position shifts towards lower energy compared with the pristine yttria, this might be due to matrix disorder through the creation of defect levels in the irradiated samples results in modification of band gap [41].

3.7. Thermoluminescence

3.7.1. Annealing effect

Annealing effect on TL properties of the Y_2O_3 NPs is investigated for improving the luminescence properties of materials. Fig. 10(a) shows TL glow curves of as prepared and annealed U:Y_2O_3 samples γ-rayed for a typical dose of 2.0 kGy. It shows the prominent TL glow with peak at 402 K. Intensity of this peak increases with increasing in annealing temperature and its glow peaks are shifted towards the lower temperature side and are shown in Fig. 10(b). Thus, 1173 K is found to be the best annealing temperature for further investigation of TL properties of Y_2O_3. Sample annealed at 1173 K shows good TL sensitivity due to improved crystallinity and reduction in the content of impurities such as –OH and C = O groups [20,43]. Similar results are reported by Mundpuzhakal et al., for CaF_2. They reported that 600 °C annealed sample shows good TL sensitivity and the shifting of peaks towards the low temperature region [44].

TL glow curves of combustion synthesized, 1173 K annealed γ-rayed U:Y_2O_3 and G:Y_2O_3 samples are shown in Fig. 11(a) and (b). Two TL glows a prominent one with peak at ~383 K (T_{m1}) and a weaker glow with peak at ~570 K (T_{m2}) are observed in U:Y_2O_3. And G:Y_2O_3 samples show glow peak at 396 K and 590 K. TL of all these samples recorded at a heating rate of 5 K s^{-1}. These peaks are attributed to oxygen vacancies such as F and F^+-centers by gamma irradiation. In our previous work, we reported TL properties of swift heavy ion (SHI) irradiated combustion synthesized Y_2O_3. A prominent and well resolved TL glow with peak at 403 K is observed along with a weak TL glow with peak at 461 K in all SHI irradiated samples [45]. In the present work, gamma irradiated U:Y_2O_3 and G:Y_2O_3 shows similar results and this is due to the fact that SHI and γ-rays induce same kinds of defects responsible for TL. Hari Krishna et al., reported TL response of UV irradiated Y_2O_3 samples prepared by ethylene diamine tetra acetic acid (EDTA) and disodium ethylene diamine tetra acetic acid (Na_2-EDTA) as fuels. EDTA based samples show a broad glow at 413 K while Na_2-EDTA based samples show a broad glow at 428 K [23]. In present work, gamma irradiated U:Y_2O_3 samples show well separated high intense low temperature glow peak (383 K) when compared to those results reported [12,13].

Fig. 12(a) and (b) shows variation of TL glow peak intensity (I_{m1}) with γ-dose for U:Y_2O_3 and G:Y_2O_3 respectively. In U:Y_2O_3 samples, it is found that TL intensity increases with increase in dose up to 6 kGy and there after it decreases with further increase in gamma (Fig. 10(a)). And, it is also found that, TL intensity linearly increases from 0.1 to 2.0 kGy (f (D) = 0.98) [22]. While in G:Y_2O_3 samples, (Fig. 12(b)) TL intensity shows sublinearity. Linearity/sublinearity and even the decrease in TL intensity of yttria at higher doses can be explained by defect interaction model (DIM) [25,46]. TL glow peak temperature values are steady in throughout the studied dose range. The increasing TL intensity with γ-doses, indicates that the electron and hole trap centers are more and hence the recombination events are increased with increase in γ-doses, which leads to increase in TL glow peak intensity [47]. The increase in TL intensity may be attributed to the creation of defect centers such as F and F^+ centers. Decrease in TL intensity with increase of γ-dose may be ascribed to the formation of complex defects [25,46]. Also, explained by the defect interaction model [46]. According to this model, at low dose, recombination within the trapping center/luminescence center (TC/LC) dominates, which leads to a linear response. The TL signal is proportional to the number of recombination occurs within the trapping entity. Further in increasing gamma dose, the separation between adjacent TC/LC complexes is reduced. Therefore, effective recombination center is high resulting in more TL signal with further increasing dose the cluster of defects is formed, resulting in decreased TL signal [46].

In order to understand the nature of the traps formed in Y_2O_3 under gamma irradiation, we have employed the analysis of trapping parameters. The evaluation of trapping parameters such as activation energy (E) of the traps involved in TL emission, order of kinetics (b), frequency factor (s) and trap density (n_o) of TL glows is one of the important aspects of TL studies. Any complete description of the TL characteristics of material requires the knowledge of these trapping parameters. Here, 'E' is the energy required for the release of the electron from the trap to reach its excited state and 's' is the rate of electron ejection. The order of kinetics 'b' is a measure of the probability that a free electron gets retrapped. This retrapping effect also depends on the availability of empty traps. The trapping parameters of TL glow curves are calculated using the glow curve shape method (modified by Chen's) [6,14]. The equations involved in glow curve shape method are given [48].

$$\mu_g = \frac{T_2 - T_m}{T_2 - T_1} \tag{6}$$

where μ_g is symmetry factor. The temperatures T_m, T_1 and T_2, are, the glow peak temperature and temperature on the lower and upper sides corresponding to half the peak intensity. The activation energy (E) is

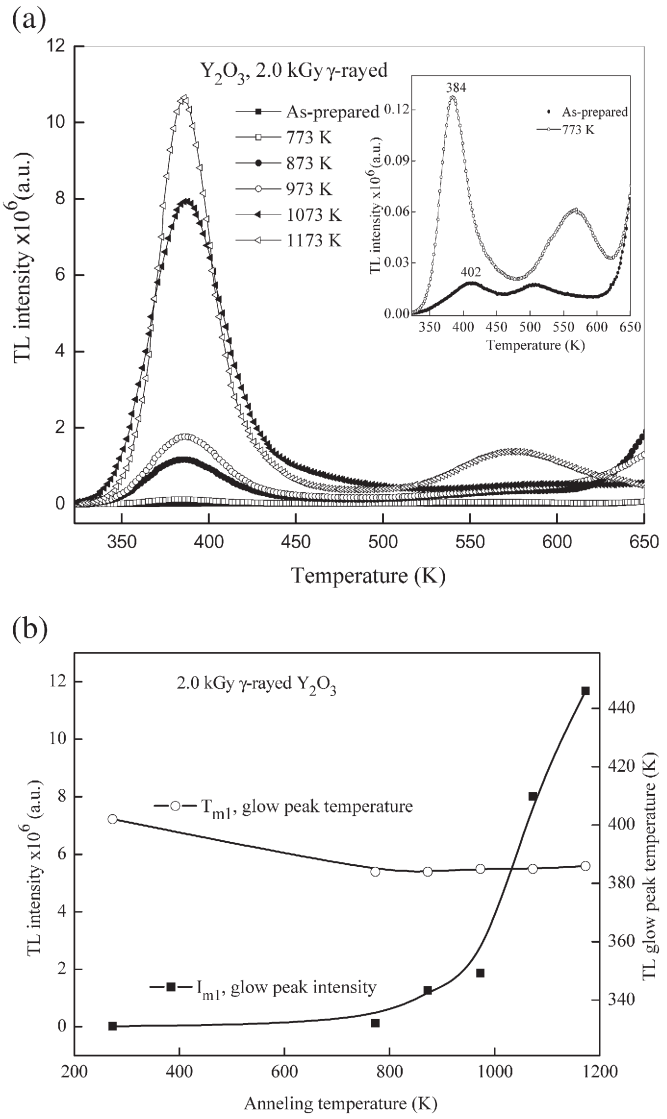

Fig. 10. (a) Thermoluminescence glow curves of combustion synthesized Y_2O_3. (b) Variation of the TL glow peak intensity and the glow peak temperature in 2.0 kGy γ-rayed Y_2O_3.

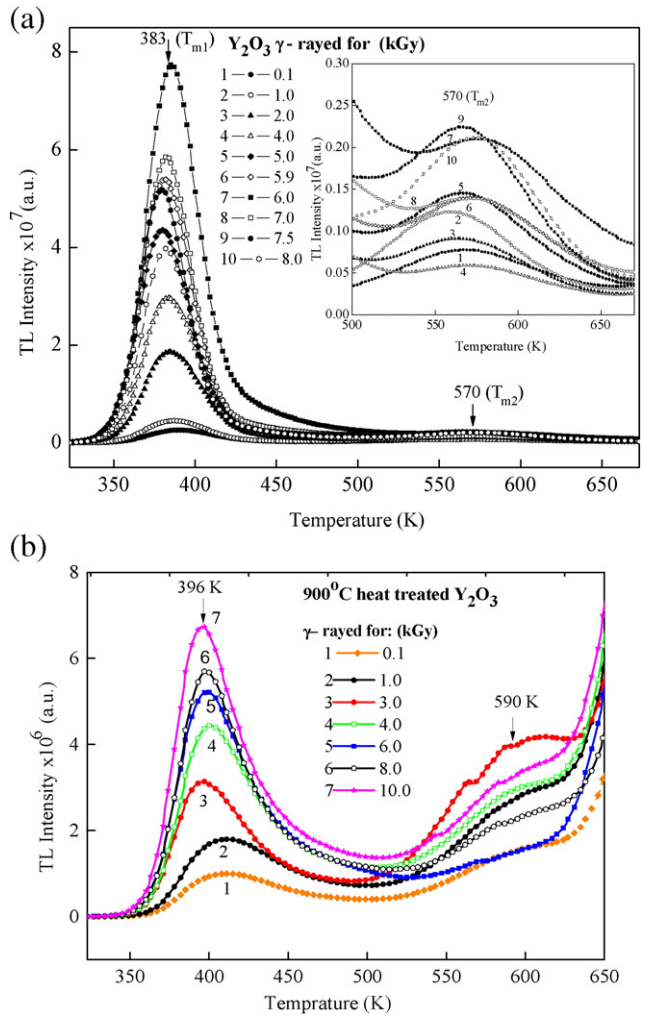

Fig. 11. (a) Thermoluminescence glow curves of combustion synthesized 1173 K annealed γ-irradiated U:Y_2O_3. (b) Thermoluminescence glow curves of combustion synthesized 1173 K annealed γ-irradiated G:Y_2O_3.

calculated using the relation

$$E_\alpha = C_\alpha \frac{kT_m^2}{\alpha} - b_\alpha (2KT_m) \tag{7}$$

where $\alpha = \tau, \delta, \omega$ with $\tau = T_m - T_1$, is the half width at the low temperature side of the peak; $\delta = T_2 - T_m$, is the half width towards the fall-off side of the glow peak and $\omega = T_2 - T_1$, is the total half width and

C_τ $1.51 + 3.0(\mu_g - 0.42)$;
b_τ $1.58 + 4.2(\mu_g - 0.42)$;
C_δ $0.976 + 7.3(\mu_g - 0.42)$;
b_δ 0;
C_ω $2.52 + 10.2(\mu_g - 0.42)$;
b_w 1.

Here, $\mu_g = \frac{\delta}{\omega}$ is called as geometrical shape factor or symmetry factor. The frequency factor is obtained from the relation

$$\frac{\beta E}{kT_m^2} = s \exp\frac{-E}{KT_m}\left[1 + (b-1)\Delta_m\right] \tag{8}$$

where $\Delta_m = \frac{2KT_m}{E}$, b is the order of kinetics, k is the Boltzmann constant (8.6×10^{-5} eV K^{-1}) and β is the linear heating rate (5 K s^{-1} in the present work).

And trap density (n_o) is calculated using the relation,

$$n_o = \frac{\omega I_m}{\beta\left\{2.52 + 10.2\left(\mu_g - 0.42\right)\right\}} \tag{9}$$

where $\omega = T_2 - T_1$, β is the heating rate and μ_g is symmetry factor.

A typical result for a glow curve of U:Y_2O_3 γ-rayed for 1.0 kGy is shown in Fig. 13(a). Theoretically, symmetry (geometrical) factor (μ_g) is close to 0.42 for first order kinetics and 0.52 for second order kinetics and in between for general order [30]. From the values of the geometrical factor it is clear that the two glows obey the second order kinetics indicating the occurrence of retrapping phenomenon. Similarly, a typical dose of 3.0 kGy γ-ray irradiated G:Y_2O_3 is deconvoluted due to overlapping of more than one glow peaks. The deconvolution of the TL glow curves in the present studies performed using computerized glow curve deconvolution (CGCD) method [49]. The deconvoluted TL glow curves are obtained for the best fit of theoretical curve with the experimental one. In the present work, theoretical fit matches with experimental data for five deconvoluted curves. The fitted TL glow curve for γ-ray irradiated G:Y_2O_3 is shown in Fig. 13(b). The glow curve of γ-ray irradiated G:Y_2O_3 can be best described as a superposition of five glow peaks at 395, 432, 483, 552 and 602 K. It indicates that five different sets of traps are involved. All deconvoluted peaks are found to obey second order kinetics. The trapping parameters of U:Y_2O_3 and G:Y_2O_3 are tabulated in Table 3.

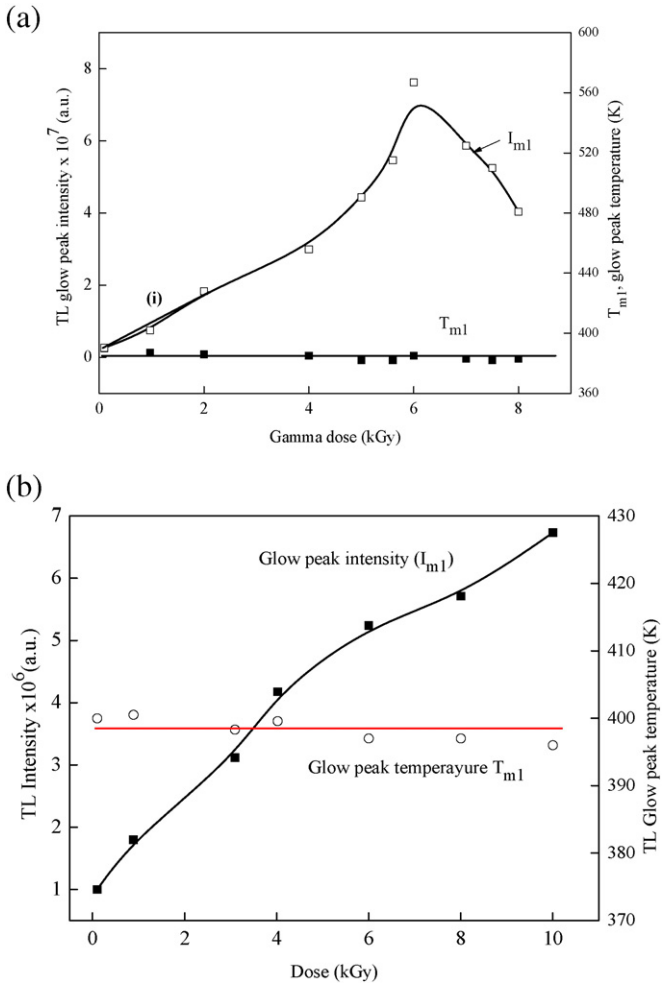

Fig. 12. (a) Variation of TL glow peak intensity (I_{m1}) and TL glow peak (Tm_1) temperature with γ-dose in U:Y_2O_3. (b) Variation of TL glow peak intensity (I_{m1}) and TL glow peak (T_{m1}) temperature with γ-dose in G:Y_2O_3.

3.7.2. Effect of heating rate on TL glow curves

Fig. 14(a) shows the effect of heating rate on the TL glow curves of a 2.0 kGy γ-ray irradiated U:Y_2O_3 NPs. The TL glow peak position (T_{m1}) shifts towards the higher temperature side with increasing heating rate whereas the glow peak intensity decreases linearly. The variation is given in Fig. 14(b). This may be attributed to thermal quenching of TL due to increase in heating rate [48]. And, the full width at half maximum (FWHM) is found to increase with heating rate. It is observed that, the activation energy and frequency factor corresponding to first (~383 K) and second TL glow peaks (~570 K) decrease with heating rate (see Table 4) and these may be attributed to the thermal quenching effect [50,51]. It may also be noted that the TL glow peak temperature and intensity depend on various parameters such as the nature of the sample such as crystalline, semicrystalline, amorphous, the impurity content, heat treatment given to the sample prior to irradiation, the nature of the ionizing radiation, the amount of irradiation (dose), temperature at which the TL measurements are made, the time interval between the measurements, the environment condition of the sample during TL measurements, the type of detector and the heating rate [14,50,51].

Table 3
Trapping parameters of TL glows in γ-irradiated U:Y_2O_3 and G:Y_2O_3.

Fuel (dose)	TL Peak	T_m (K)	μ_g	Order of kinetics	E (eV)	s (s^{-1})	Trap density no (cm^{-3})
Urea	T_{m1}	385	0.52	2	0.979	2.17×10^{12}	1.120×10^{7}
(1 kGy)	T_{m2}	563	0.49	2	0.720	4.36×10^{9}	1.210×10^{7}
Glycine	T_{m1}	395	0.52	2	1.15	1.88×10^{14}	1.41×10^{7}
(3 kGy)	T_{m2}	432	0.51	2	1.17	1.51×10^{13}	6.03×10^{6}
	T_{m3}	483	0.51	2	1.20	9.46×10^{11}	1.12×10^{6}
	T_{m4}	552	0.50	2	1.25	5.81×10^{10}	7.27×10^{6}
	T_{m5}	602	0.50	2	1.30	1.51×10^{10}	3.03×10^{7}

3.7.3. Fading

To study the effect of fading on TL glow curves of U:Y_2O_3 and G:Y_2O_3, samples are exposed for a test dose of 6.0 kGy. Fig. 15 shows the plot of normalized TL intensity as a function of storage time after γ-irradiation [51]. It is found that there is 20% and 22% fading over a period of sixty days for U:Y_2O_3 and G:Y_2O_3 samples respectively. The fading is observed

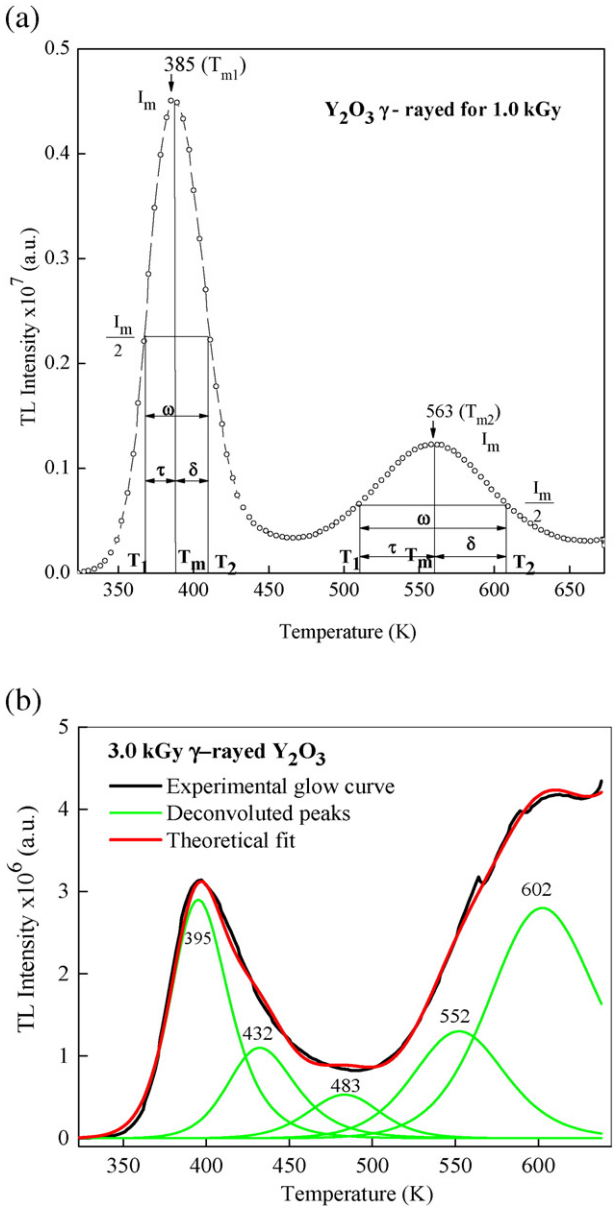

Fig. 13. (a) Glow curve deconvolution of U:Y_2O_3 exposed to 1.0 kGy γ-radiation. (b) Glow curve deconvolution of G:Y_2O_3 exposed to 3.0 kGy γ-radiation.

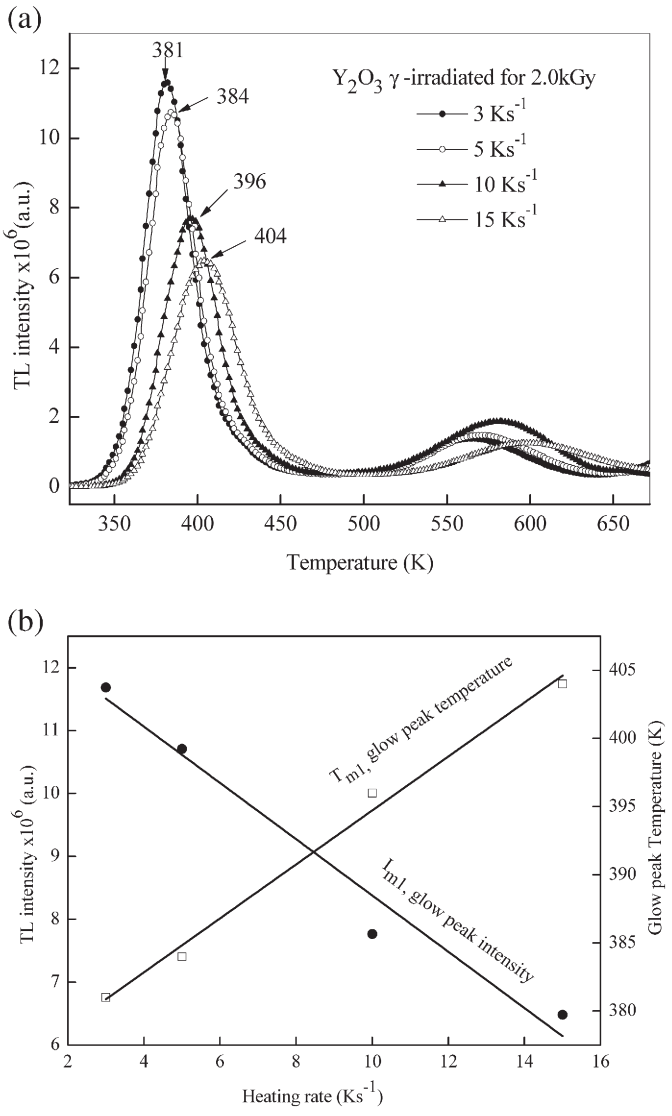

Fig. 14. (a) Effect of heating rate on the TL glow curves of U:Y_2O_3. (b) Variation of TL glow peak intensity and glow peak temperature with heating rate on the TL glow curves of U:Y_2O_3.

Table 4
Trapping parameters of TL glows of U:Y_2O_3 recorded at different heating rate.

Heating rate ($K\ s^{-1}$)	Peaks	T_m (K)	μ_g	Order of kinetics	Activation energy (eV)	Frequency factor (s^{-1})	Trap density (cm^{-3})
3	T_{m1}	381	0.52	2	1.289	5.97×10^{16}	2.06×10^{7}
	T_{m2}	565	0.52	2	1.432	1.54×10^{12}	3.50×10^{6}
5	T_{m1}	384	0.52	2	1.033	1.25×10^{13}	4.22×10^{7}
	T_{m2}	568	0.52	2	0.906	1.97×10^{7}	4.65×10^{6}
10	T_{m1}	396	0.49	2	1.045	7.71×10^{12}	1.77×10^{7}
	T_{m2}	581	0.47	2	1.061	2.78×10^{8}	6.98×10^{6}
15	T_{m1}	404	0.51	2	0.930	1.30×10^{11}	1.72×10^{7}
	T_{m2}	601	0.49	2	1.065	1.39×10^{8}	4.48×10^{6}

to be very high initially (~14% in decrease during first five days) and later the fading becomes slow.

Further, the TL results of the present work are compared with reported TL dosimetric properties of $CaSO_4:Dy^{3+}$ (TLD-900). TLD-900 exhibits glow peak at high temperature (~494 K) with a weak shoulder at ~415 K [52,53]. Y_2O_3 exhibit a well resolved prominent TL glow peak at 383 K and weak one at 570 K. 383 K shows relatively high intensity, good stability and responds to γ-doses. Further, Y_2O_3 shows the linearity in the γ-dose range 0.1–2.0 kGy where as $CaSO_4:Dy^{3+}$ shows the linearity in the dose range 0.5–1.0 kGy [52]. However, a detailed investigation needs to be carried out on Y_2O_3 for its suitability in radiation dosimetry.

4. Conclusions

Nanocrystalline Y_2O_3 is synthesized by combustion technique using urea and glycine as fuels. The X-ray diffraction pattern confirms the cubic phase. The average crystallite size is found to be ~29.42 nm. FTIR spectra confirmed the purity of the synthesized sample. The FE-SEM picture of annealed Y_2O_3 shows well separated spherical shape particles with average particle size ~35 nm. Raman spectra confirm the cubic bixbyite structure of Y_2O_3. ESR spectrum of γ-irradiated U:Y_2O_3 confirmed the oxygen vacancy related defects and Y^{2+} defects. The energy gap of the synthesized samples is found to be 5.2 and 5.1 eV for U:Y_2O_3 and G:Y_2O_3 respectively. Broad PL emission with peaks around 386, 440, 486 and 538 nm is observed in the synthesized samples and these peaks are attributed to F, and F^+ centers and Y^{3+}–O^{2-} donor acceptor pairs respectively. The TL kinetic parameters are calculated using glow curve shape method. TL glow curves of γ-irradiated U:Y_2O_3 and G:Y_2O_3 samples exhibit second order kinetics. It is noticed that urea based Y_2O_3 samples exhibit high TL intensity with linear response and less fading. And, such materials are quite suitable for applications in high radiation environments.

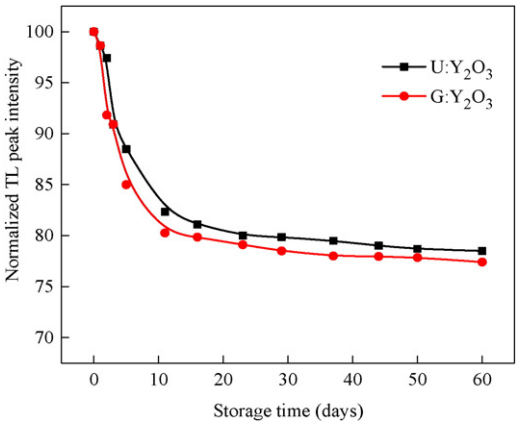

Fig. 15. Effect of fading with number of days in U:Y_2O_3 and G:Y_2O_3 nanocrystal.

Acknowledgments

The authors express their sincere thanks to Dr. D.K. Avasthi, Senior Scientist, Materials Science Group, and Dr. S.P. Lochab, Health Physics Group, Inter University Accelerator Centre, New Delhi, India for their constant encouragement and help during the experiment. And, authors are thankful to Dr. S.V. Bhat, Senior Scientist, Department of Physics, Indian Institute of Science, Bangalore for providing ESR facilities. Also, one of the authors (NJS) is grateful to Inter University Accelerator Centre, New Delhi, for providing fellowship under UFR (No. 48303) scheme.

References

[1] C. Pandurangappa, B.N. Lakshminarasappa, Opt. Commun. 285 (2012) 2739–2742.
[2] M. Sekita Fukabori, T. Ikegami, N. Iyi, T. Komatsu, M. Kawamura, M. Suzuki, J. Appl. Phys. 101 (2007) 043112.
[3] J.Q. Xu, S.J. Xiong, X.L. Wu, T.H. Li, J.C. Shen, P.K. Chu, J. Appl. Phys. 114 (2013) 093512.
[4] L. Robindro Singh, R.S. Ningthoujam, V. Sudarsan, I. Srivastava, S. Dorendrajit Singh, G.K. Dey, et al., Nanotechnology. 19 (2008) 055201.
[5] B.N. Lakshminarasappa, N.J. Shivaramu, K.R. Nagabhushana, F. Singh, Nucl. Instruments Methods Phys. Res. Sect. B Beam Interact. with Mater. Atoms 329 (2014) 40–47.
[6] N. Salah, P.D. Sahare, S.P. Lochab, P. Kumar, Radiat. Meas. 41 (2006) 40–47.
[7] H. Yang, F. Peng, Q. Zhang, W. Liu, D. Sun, Y. Zhao, et al., Opt. Mater. (Amst) 35 (2013) 2338–2342.
[8] L. Li, M. Zhao, W. Tong, X. Guan, G. Li, L. Yang, Nanotechnology. 21 (2010) 195601.
[9] G.T. Chandrappa, R. Gopichandran, K.C. Patil, Int. J. Self-Propag. High-Temp. Synth. 183 (1995) 4–12.
[10] L. Wang, Y. Pan, Y. Ding, W. Yang, W.L. Mao, S.V. Sinogeikin, Y. Meng, G. Shen, H. Mao, Appl. Phys. Lett. 94 (2009) 061921.
[11] T. Mimani, K.C. Patil, Mater. Phys. Mech. 4 (2001) 134–137.
[12] S. Mukherjee, V. Sudarsan, P.U. Sastry, a.K. Patra, a.K. Tyagi, J. Lumin, 145 (2014) 318–323.
[13] G. Ramakrishna, H. Nagabhushana, D.V. Sunitha, S.C. Prashantha, S.C. Sharma, B.M. Nagabhushana, Spectrochim. Acta. A. Mol. Biomol. Spectrosc. 127 (2014) 177–184.
[14] R. Chen, S.W.S. McKeever, Theory of thermoluminescence and related phenomena, World Scientific, Singapore, 1997.
[15] N. Salah, P.D. Sahare, A.A. Rupasov, J. Lumin. 124 (2007) 357–364.
[16] M.S. Zhang, Z. Yin, Phys. Status Solidi 179 (2000) 319.
[17] M. Mitric, A. Kremenovic, R. Dimitrijevic, D. Rodic, Solid State Ionics 101 (1997) 495–501.
[18] N.F.P. Ribeiro da Silva, M.M.V.M. Souza, Ceram. Int. 35 (2009) 3441–3446.
[19] J. McKittrick, L.E. Shea, C.F. Bacalski, E.J. Bosze, Displays. 19 (1999) 169–172.
[20] W.H. Khorsand Zak, Abd Majid, M.E. Abrishami, Ramin Yousefi, Solid State Sci. 13 (2011) 251–256.
[21] B.D. Cullity, Elements of X-ray diffraction, 2nd ed. Addison-Wesley publishing company, Inc. USA, Reading, MA, 1956.
[22] S. Som, S. Datta, M. Chowdhury, Vijay Kumar, Vinod Kumar, H.C. Swart, S.K. Sharma, J. Alloys compd. 589 (2014) 5–18.
[23] R. Hari Krishna, B.M. Nagabhushana, H. Nagabhushana, R.P.S. Chakradhar, R. Sivaramakrishna, C. Shivakumara, et al., J. Alloys Compd. 585 (2014) 129–137.
[24] R. Subramanian, P. Shankar, S. Kavithaa, S.S. Ramakrishnnan, P.C. Angelo, Mater. Latt. 48 (2001) 342–346.
[25] N.J. Shivaramu, B.N. Lakshminarasappa, K.R. Nagabhushana, Radiat. Meas. 71 (2014) 518–523.
[26] R.V. Mangalaraja, J. Mouzon, P. Hedstrom, CarlosP. , S. Camurri, M. Ananthakumar, Oden, Powder Technol. 191 (2009) 309–314.
[27] Faheem Ahmed, Shalendra Kumar, Nishat Arshi, M.S. Anwar, Bon Heun Koo, Chan Gyu Le, Microelectron. Eng. 89 (2012) 129–132.
[28] S. Bhagavantam, T. Venkataryudu, Proc.-Indian Acad. Sci., Sect. A 9 (1939) 224–226.
[29] Sudeshna Ray, Sergio Fabian Leon-Luis, Francisco Javier Manjon, Miguel Alfonso Mollar, Oscar Gomis, Ulises Ruyman Rodríguez-Mendoza, Said Agouram, Alfonso Munoz, Victor Lavin, Cur. Appl. Phys. 14 (2014) 72–81.
[30] Jian Zuo, Cunyi Xu, Yunpiug Liu, Yitai Qian, Nanostntdured Materials 10 (1998) 1331–1335.
[31] Y. Osada, S. Koike, T. Fukushima, S. Ogasawara, Applied Catalysis 59 (1990) 59–74.
[32] J. Wang, H. Song, Baojun Sun, Xinguang Ren, Baojiu Chen, Wu Xu, Chemical Physics Letters 379 (2003) 507–511.
[33] R. HariKrishna, B.M. Nagabhushana, H. Nagabhushana, D.L. Monika, R. Sivaramakrishna, C. Shivakumara, R.P.S. Chakradhar, Tiju Thomas, J. Lumin. 155 (2014) 125–134.
[34] Xiaolin Liu, Feng Zhou, Mu Gu, Shiming Huang, Bo Liu, Chen Ni, Opt. Mater. 31 (2008) 126–130.
[35] G. Liu, G. Hong, X. Dong, J. Wang, J. Lumin. 126 (2007) 702–706.
[36] O.M. Bordun, j. Appl. Spectr. 69 (2002) 430–433.
[37] V.V. Osipov, a.V. Rasuleva, V.I. Solomonov, Opt. Spectrosc. 105 (2008) 524–530.
[38] E. Souza, G.T.A. Santos, B.C. Barra, W.D. Macedo, S.R. Teixeira, C.M. Santos, A.M.O.R. Senos, L. Amaral, E. Longo, Cryst. Growth Des. 12 (2012) 5671–5679.
[39] K. Gayatri Sharma, N. Shanta Singh, Y. Rangeela Devi, N. Rajmuhon Singh, Sh. Dorendrajit Singh, J. Alloy Comp. 556 (2013) 94–101.

[40] V. Kumar, R.G. Sonkawade, S.K. Chakarvarti, P. Kulriya, K. Kant, N.L. Singh, et al., Vacuum. 86 (2011) 275–279.
[41] M.F. Zaki Tayel, A.B. El Basaty, T.M. Hegazy, J. Adv. Res. (2014) (In press).
[42] T.K. Srinivasan, B.S. Panigrahi, a.K. Arora, B. Venkatraman, D. Ponraju, Radiat. Phys. Chem. 99 (2014) 92–96.
[43] N. Salah, S.S. Habib, Z.H. Khan, F. Djouider, Radiat. Phys. Chem. 80 (2011) 923–928.
[44] J.K. Mundupuzhakal, R.H. Biswas, S. Chauhan, V. Varma, Y.B. Acharya, B.S. Chakrabarty, Radiation Protection Dosimetry (2014) 1–6.
[45] G. Szenes, Phys. Rev. B. 60 (1999) 3140–3147.
[46] S. Mahajna, Y.S. Horowitz, J. Phys. D: Appl. Phys. 30 (1997) 2603–2619.
[47] Numan Salah, Sami.S. Habib, ZishanH .Khan, SalimAl -Hamedi, S.P. Lochab, J. Lumin. 129 (2009) 192–196.
[48] N.J. Shivaramu, B.N. Lakshminarasappa, K.R. Nagabhushana, F. Singh, Radiat. Eff. Defects Solids. 169 (2014) 696–705.
[49] D. Afouxenidis, G.S. Polymeris, N.C. Tsirliganis, G. Kitis, Radiat. Protection Dosimetry 149 (2012) 363–370.
[50] R. Chen, J. Electrochem. Soc. 116 (1969) 1254–1257.
[51] C. Furetta, Handbook of Thermoluminescence. , World Scientific Publishing, Singapore, 1937.
[52] B. Sanyal, V. Natarajan, S.P. Chawla, A. Sharma, Radiat. Meas. 45 (2010) 899–905.
[53] N. Salah, P.D. Sahare, J. Phys. D. Appl. Phys. 39 (2006) 2684–2691.